Translation of the intrinsically disordered protein α-synuclein is inhibited by a small molecule targeting its structured mRNA

Peiyuan Zhang[a,1], Hye-Jin Park[b,c,1], Jie Zhang[b,c], Eunsung Junn[b,c], Ryan J. Andrews[d], Sai Pradeep Velagapudi[a], Daniel Abegg[a], Kamalakannan Vishnu[a], Matthew G. Costales[a], Jessica L. Childs-Disney[a], Alexander Adibekian[a], Walter N. Moss[d], M. Maral Mouradian[b,c,2], and Matthew D. Disney[a,2]

[a]Department of Chemistry, The Scripps Research Institute, Jupiter, FL 33458; [b]Rutgers Robert Wood Johnson Medical School Institute for Neurological Therapeutics, Rutgers Robert Wood Johnson Medical School, Piscataway, NJ 08854; [c]Department of Neurology, Rutgers Robert Wood Johnson Medical School, Piscataway, NJ 08854; and [d]Roy J. Carver Department of Biophysics, Biochemistry and Molecular Biology, Iowa State University, Ames, IA 50011

Edited by Daniel Herschlag, Stanford University, Stanford, CA, and approved November 26, 2019 (received for review March 28, 2019)

Many proteins are refractory to targeting because they lack small-molecule binding pockets. An alternative to drugging these proteins directly is to target the messenger (m)RNA that encodes them, thereby reducing protein levels. We describe such an approach for the difficult-to-target protein α-synuclein encoded by the *SNCA* gene. Multiplication of the *SNCA* gene locus causes dominantly inherited Parkinson's disease (PD), and α-synuclein protein aggregates in Lewy bodies and Lewy neurites in sporadic PD. Thus, reducing the expression of α-synuclein protein is expected to have therapeutic value. Fortuitously, the *SNCA* mRNA has a structured iron-responsive element (IRE) in its 5′ untranslated region (5′ UTR) that controls its translation. Using sequence-based design, we discovered small molecules that target the IRE structure and inhibit *SNCA* translation in cells, the most potent of which is named Synucleozid. Both in vitro and cellular profiling studies showed Synucleozid directly targets the α-synuclein mRNA 5′ UTR at the designed site. Mechanistic studies revealed that Synucleozid reduces α-synuclein protein levels by decreasing the amount of *SNCA* mRNA loaded into polysomes, mechanistically providing a cytoprotective effect in cells. Proteome- and transcriptome-wide studies showed that the compound's selectivity makes Synucleozid suitable for further development. Importantly, transcriptome-wide analysis of mRNAs that encode intrinsically disordered proteins revealed that each has structured regions that could be targeted with small molecules. These findings demonstrate the potential for targeting undruggable proteins at the level of their coding mRNAs. This approach, as applied to *SNCA*, is a promising disease-modifying therapeutic strategy for PD and other α-synucleinopathies.

RNA | chemical biology | Parkinson's disease | α-synuclein | intrinsically disordered proteins

Human diseases are often caused by malfunctioning proteins with diverse functions, and yet only a small set of them can be drugged or targeted with a small molecule (1, 2). Indeed, a genome-wide analysis showed that only 15% of proteins are considered to be in druggable protein families, while the remaining 85% are considered "undruggable" (1, 2). Many of these undruggable proteins do not fold into defined structures or assume structures lacking pockets suitable for binding small molecules (3, 4). One intriguing strategy to expand protein druggability, particularly for proteins with aberrantly high levels linked to disease, is to target their encoding mRNAs and inhibit translation. Such an approach could be accomplished by defining structured regions in an mRNA, namely potential small-molecule binding pockets, and then identifying lead small molecules that bind these structures, that is, a sequence-based design strategy. Indeed, we have previously used such an approach to target RNA broadly, including primicroRNAs (miRNAs), pre-miRNAs, and mRNAs (5, 6).

α-Synuclein is a key protein in the pathogenesis of Parkinson's disease (PD) and other α-synucleinopathies based on genetics, neuropathology, cell biology, and animal model studies (7). This protein can oligomerize, misfold, and form fibrils that propagate across neurons in the brain and accumulate in Lewy bodies and Lewy neurites (8, 9). The expression level of α-synuclein is an important determinant of the rate of its fibrillization and neurotoxicity (10, 11), as individuals with multiplication of the *SNCA* gene locus develop dominantly inherited PD and dementia with a gene-dosage effect (12). Additionally, polymorphisms in the promoter region and in a distal enhancer element of the *SNCA* gene impact α-synuclein protein levels and elevate the risk of developing PD (13–15). Thus, reducing the expression level of this protein is expected to be a disease-modifying strategy (16, 17) (Fig. 1*A*).

α-Synuclein is an intrinsically disordered protein (IDP) and is therefore difficult to target, owing to its lack of defined small-molecule binding pockets. At the RNA level, however, *SNCA* mRNA displays a functionally important and structured 5′ untranslated region (UTR) with an iron-responsive element (IRE) that regulates its translation (Fig. 1 *A* and *B*) (18, 19). The IRE is bound by iron regulatory protein (IRP) at low concentrations of iron. At high concentrations, IRP is bound by iron, freeing the

Significance

Parkinson's disease and its associated dementia can be caused by elevated levels of α-synuclein protein. Despite many efforts, however, targeting α-synuclein at the protein level has been challenging. In this manuscript, we describe the design of a small molecule that selectively targets the messenger RNA that encodes α-synuclein protein and selectively inhibits its translation. Furthermore, the compound is cytoprotective. Collectively, our findings show that difficult-to-target proteins can indeed be regulated by small molecules by binding the encoding mRNA. This strategy is a potentially promising way to slow the progression of Parkinson's disease and related neurological disorders.

Author contributions: J.L.C.-D., W.N.M., M.M.M., and M.D.D. designed research; P.Z., H.-J.P., J.Z., E.J., R.J.A., S.P.V., D.A., K.V., M.G.C., and A.A. performed research; P.Z., H.-J.P., J.Z., E.J., R.J.A., S.P.V., D.A., K.V., M.G.C., A.A., W.N.M., M.M.M., and M.D.D. analyzed data; and P.Z., J.L.C.-D., M.M.M., and M.D.D. wrote the paper.

Competing interest statement: M.D.D. is a founder of Expansion Therapeutics.

This article is a PNAS Direct Submission.

Data deposition: RNA-seq data are available in the Gene Expression Omnibus (GEO) repository (accession no. GSE129590). Data related to the structures of mRNAs that encode IDPs are available in the Zenodo repository (DOI: 10.5281/zenodo.3594202).

[1]P.Z. and H.-J.P. contributed equally to this work.

[2]To whom correspondence may be addressed. Email: m.mouradian@rutgers.edu or disney@scripps.edu.

This article contains supporting information online at https://www.pnas.org/lookup/suppl/doi:10.1073/pnas.1905057117/-/DCSupplemental.

First published January 3, 2020.

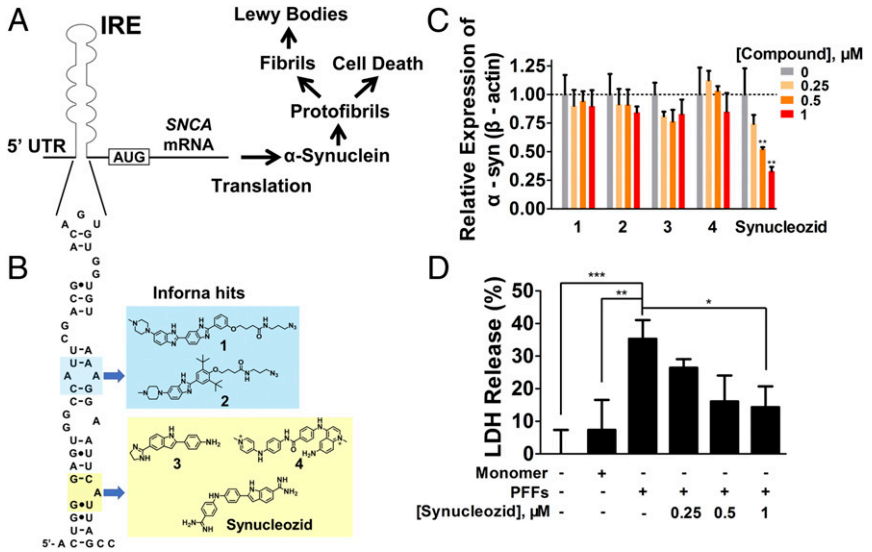

Fig. 1. Design and characterization of an *SNCA* 5′ UTR IRE-targeting small molecule. (*A*) Schematic depiction of an α-synuclein–mediated disease pathway. (*B*) Secondary structure of the 5′ UTR IRE of *SNCA* mRNA that regulates translation and the chemical structures of hit small molecules predicted by Infornа. (*C*) Quantification of a Western blotting screen of candidate small molecules inhibiting α-synuclein protein expression in SH-SY5Y neuroblastoma cells. (*D*) Cytoprotective effect of Synucleozid against α-synuclein toxicity in SH-SY5Y cells measured using a lactate dehydrogenase assay. Synucleozid abrogates cytotoxicity induced by α-synuclein preformed fibrils, which act as seeds and recruit endogenous α-synuclein to aggregate. $*P < 0.05$, $**P < 0.01$, $***P < 0.001$, as determined by ANOVA. Error bars indicate SD.

mRNA to undergo translation (20, 21). The presence of iron in Lewy bodies and translational control of α-synuclein via iron and the IRE support their collective roles in PD (22, 23).

Thus, small molecules that target this RNA structure could be of value as probes that inhibit translation of α-synuclein, enabling the study of associated pathogenetic mechanisms. Further, such studies could provide new strategies for drugging undruggable proteins by targeting them at the RNA level. We therefore employed our sequence-based design, lead-identification strategy, Infornа (5, 24), to target the *SNCA* IRE. Infornа is built around a database of experimentally determined, privileged RNA fold–small molecule interactions. That is, the interactions are both high-affinity and selective. Infornа then searches an RNA target for druggability, that is, whether it houses an RNA fold in the database. The small molecules that bind this targetable fold are lead chemical probes that can be assessed for biological effects. Indeed, Infornа has defined highly selective lead small molecules that target many RNAs from different classes, modulating their biology in highly predictable, rational ways in both cellular and preclinical animal models (6, 25, 26).

In the present study, Infornа provided a cohort of small molecules that bind folds present in the *SNCA* IRE. The most effective compound, named Synucleozid, selectively repressed α-synuclein translation in a neuronal cell line, as determined by proteome-wide studies, providing a cytoprotective effect. Cellular mechanistic studies revealed that Synucleozid: 1) binds and stabilizes the *SNCA* IRE in cells at a specific structural element, as designed by Infornа, and 2) represses translation by stabilizing the IRE, thereby causing an accumulation of ribosome precursors on the mRNA and hence reducing the amount of *SNCA* mRNA loaded into polysomes. The former mechanistic studies were enabled by an approach we developed to study molecular recognition of RNAs by small molecules both in vitro and in cells, dubbed antisense oligonucleotide ligand binding site mapping (ASO-Bind-Map) (27). ASO-Bind-Map will likely have broad utility as a target-validation tool as the field of RNA-targeted small molecules grows. Additionally, in silico results presented here suggest that, in addition to *SNCA*, structured RNA elements are predicted to form in the mRNAs of all IDPs—with some having extensive structure and multiple (potentially targetable) motifs. Thus, the approaches described herein could be broadly applicable.

Results and Discussion

Design of Compounds Targeting the *SNCA* IRE. The translation of some α-synuclein isoforms is regulated by a 3-dimensionally folded hairpin structure that is similar to IREs in the 5′ UTR in its encoding mRNA (located in exon 1 upstream of the AUG start codon; Fig. 1 *A* and *B*) (18, 21). To determine the percentage of *SNCA* mRNA transcripts harboring the IRE, we performed RNA-seq (sequencing) analysis of SH-SY5Y cells, a human dopaminergic neuroblastoma cell line commonly used to study the expression of α-synuclein. Of the 13 *SNCA* mRNA transcripts (28), 5 transcripts passed the detection criteria for further analysis [at least 5 estimated counts in at least 47% of the samples (29); *SI Appendix*, Table S1]. Among these 5 transcripts, 2 (transcripts SNCA-204 and SNCA-205) contain the targeted IRE sequence. SNCA-204 and SNCA-205 make up ∼50% of all *SNCA* mRNA species in SH-SY5Y cells (*SI Appendix*, Table S1). Therefore, this IRE-like hairpin is an attractive therapeutic target to reduce α-synuclein protein levels.

To explore such a strategy, we sought to design small molecules that bind the *SNCA* 5′ UTR IRE structure. Two different models of the *SNCA* 5′ UTR IRE structure have been reported in the literature, deduced from free-energy minimization and/or comparative sequence analysis (18, 21, 30). Here, we have used a combined approach of evolutionary conservation and free-energy minimization to refine the structure. The resulting model (Fig. 1*B*) is further supported by its structural conservation (91.6%) and the observation of multiple structure-preserving mutations in homologous *SNCA* sequences—spanning eutherian mammals, as explored using Rfam (31) (*SI Appendix*, Fig. S1). The structure is similar to that reported by Rogers et al. (30), except that the helix adjacent to the hairpin is slipped, affording remarkable similarity between the human *SNCA* and ferritin IRE structures. Interestingly, a potential compensatory mutation was identified in our conservation studies, supporting the revised model helix (*SI Appendix*, Fig. S1*A*). In vitro mapping studies support that the 2 models may be in equilibrium (*SI Appendix*, Fig. S1*B*). Our lead-identification strategy, Infornа (5, 24), then identified 5 compounds that are privileged for 2

structural elements found in both models of the IRE, namely a 1 × 1–nucleotide internal loop and a 1-nucleotide bulge with GC and GU closing base pairs (Fig. 1*B*).

To investigate the likelihood that these structures form within IRE-containing species, we evaluated the sequence conservation of their closing base pairs (*SI Appendix*, Fig. S1*A*) as well as sequence variation as reported in *SI Appendix*, Fig. S1*C*. The 1-nucleotide bulge's closing pairs are 100% conserved in a MAFFT alignment of 55 sequences of eutherian mammals while 1 closing base pair of the internal loops is conserved 100% and the other <90% (*SI Appendix*, Fig. S1*A*). To further investigate the sequence variation within the *SNCA* IRE, we queried the NCBI database and found that the highest-population minor-allele frequency (MAF) observed in any population, including 1000 Genomes phase 3, ESP, and gnomAD, is equal to or less than 0.01 for all nucleotides, indicating high sequence conservation of the *SNCA* IRE (*SI Appendix*, Fig. S1*C*) (28).

As a first assessment of activity, the compounds were studied for inhibiting α-synuclein translation in SH-SY5Y cells (Fig. 1*C*). Of these, Synucleozid, designed to bind the A bulge near the base of the IRE hairpin, reduced levels of α-synuclein in a dose-dependent manner with an IC_{50} of ∼500 nM (Fig. 1*C* and *SI Appendix*, Fig. S2). To ensure that reduction of protein levels was due to inhibition of translation and not transcription, *SNCA* mRNA levels were measured by reverse transcription-quantitative real-time PCR (RT-qPCR) upon compound treatment. Indeed, Synucleozid had no effect on the steady-state levels of *SNCA* mRNA (*SI Appendix*, Fig. S3). In agreement with these cellular studies on endogenous α-synuclein protein and mRNA levels, Synucleozid inhibited α-synuclein translation using a luciferase construct fused to the *SNCA* 5′ UTR, both in transfected SH-SY5Y cells (Fig. 2*A*) and in vitro (*SI Appendix*, Fig. S4). Dose-dependent effects were observed in both systems, with 1 μM Synucleozid inhibiting ∼40% of translation in cells. No inhibitory effect (cellular or in vitro) was observed for a construct in which the *SNCA* 5′ UTR was absent (Fig. 2*A* and *SI Appendix*, Fig. S4). Importantly, no toxicity was observed upon Synucleozid treatment of SH-SY5Y cells, as determined by cell viability (3-(4,5-dimethylthiazol-2-yl)-5-(3-carboxymethoxyphenyl)-2-(4-sulfophenyl)-2H-tetrazolium [MTS]) and lactate dehydrogenase (LDH) release (*SI Appendix*, Fig. S5).

To assess the biological effect of Synucleozid on an α-synuclein–mediated phenotype, we studied its ability to confer cytoprotection against the toxicity of α-synuclein preformed fibrils (PFFs) (32). The PFFs are composed of recombinant human α-synuclein that, when delivered to cells, seeds the aggregation and fibrillization of soluble endogenous α-synuclein, triggering downstream cellular damage and toxicity that can be measured by LDH release. As expected for a compound that reduces levels of α-synuclein, Synucleozid mitigated the toxicity induced by PFFs in a concentration-dependent manner (Fig. 1*D*). Because of these favorable cellular properties of Synucleozid, we completed in-depth analysis of this compound and derivatives thereof to establish its mechanism of action and confirmed its direct engagement of the *SNCA* IRE.

Selectivity of Synucleozid for the *SNCA* IRE. *SNCA* is not the sole mRNA expressed in the nervous system that contains an IRE in its 5′ UTR. We therefore studied whether Synucleozid also inhibits translation of these mRNAs, including amyloid precursor protein (APP), prion protein (PrP), and ferritin. We created analogous luciferase reporter gene constructs for the APP, PrP, and ferritin 5′ UTRs (Fig. 2*A*, *Top* and *SI Appendix*, *Methods*) and studied the effect of Synucleozid on their translation in SH-SY5Y cells. In contrast to the luciferase reporter fused to the *SNCA* 5′ UTR, Synucleozid had no effect on translation of luciferase fused to the APP or PrP 5′ UTRs. A very small (∼10% inhibition) but statistically significant effect was observed for ferritin upon treatment with 1 μM Synucleozid (similar to the percent inhibition observed for the *SNCA* 5′ UTR at a 4-fold lower concentration, 250 nM) (Fig. 2*A*, *Bottom*). It is not surprising that Synucleozid is selective for the *SNCA* 5′ UTR, as the 4 UTRs studied have different secondary structures (*SI Appendix*, Fig. S6).

Considering these positive results using luciferase constructs, the endogenous levels of APP, PrP, and ferritin were measured in SH-SY5Y cells upon Synucleozid treatment. In addition, we also studied the effect of the small molecule on the transferritin receptor (TfR) as it contains an IRE in its 3′ UTR (33) and because of its role in regulating the translation of mRNAs with IREs in their 5′ UTRs (21). Mirroring the results observed using luciferase constructs, Synucleozid had no effect on protein levels of APP, PrP, or TfR (Fig. 2*B* and *SI Appendix*, Fig. S2). Although no dose–response was observed for its effect on ferritin, its levels were reduced by ∼50% at the highest concentration tested (1 μM; Fig. 2*B* and *SI Appendix*, Fig. S2). This reduction in ferritin levels could be due to an off-target effect and/or rescue of autophagic and lysosomal dysfunction observed in PD. This dysfunction has been linked to α-synuclein accumulation and α-synuclein–mediated disruption of hydrolase trafficking (34). As long-lived proteins, including ferritin, are degraded in the lysosome, rescue of lysosomal function by Synucleozid may account, in part, for reduction of ferritin levels. In support of this notion, a study in α-synuclein$^{-/-}$ mice showed that α-synuclein impaired ferritinophagy and conversely that elimination of α-synuclein reduced ferritin levels (35).

Studying Compound Affinity and Characterizing Its Binding Site within the *SNCA* IRE. Next, we measured the affinity of Synucleozid for its putative binding site in the IRE, the A bulge, by replacing the

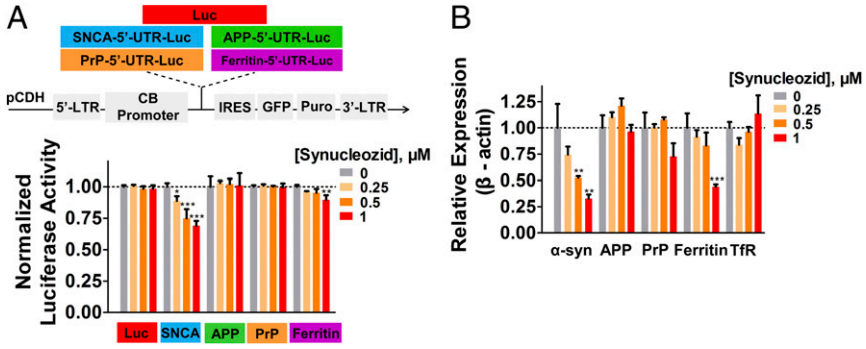

Fig. 2. Synucleozid shows on-target effects in cells. (*A*, *Top*) Structures of designed luciferase (Luc) reporter plasmids used in selectivity studies. (*A*, *Bottom*) Luciferase assay of Synucleozid effects in SH-SY5Y cells stably transduced with plasmids containing the 5′ UTR of *SNCA*, amyloid precursor protein, prion protein, or ferritin mRNAs. (*B*) Selectivity of Synucleozid for inhibiting α-synuclein protein translation as compared with its effect on APP, PrP, ferritin, and transferrin receptor determined by Western blotting. **P* < 0.05, ***P* < 0.01, ****P* < 0.001, as determined by ANOVA. Error bars indicate SD.

bulge with the fluorescent adenine mimic 2-aminopurine (2-AP) (Fig. 3*A*). The emission of 2-AP changes based on its microenvironment, particularly if it is stacked on neighboring bases (36), which can be altered upon ligand binding (37, 38). Indeed, Synucleozid decreased 2-AP emission with an EC_{50} of 2.7 ± 0.4 μM (Fig. 3*B*). Importantly, recovery of 2-AP emission was observed as a function of unlabeled *SNCA* IRE RNA (RNA-0) concentration, affording a competitive K_d of 1.5 ± 0.3 μM (Fig. 3*C* and *SI Appendix*, Fig. S7*A*). That is, both 2-AP–labeled and native IRE RNA bind to Synucleozid with similar affinities. Therefore, 2-AP–labeled IRE RNA can serve as a useful model to assess Synucleozid binding and avidity.

To converge on the A bulge as Synucleozid's binding site, competitive binding assays were completed with a series of unlabeled RNAs into which mutations were introduced (Fig. 3*C* and *SI Appendix*, Fig. S8) and 2-AP–labeled IRE RNA. For these investigations, each noncanonically paired region was systematically replaced with base pairs, generating RNA-1 to RNA-5 (Fig. 3*C* and *SI Appendix*, Fig. S8). Additionally, we completed a mutational analysis for the A bulge and its surrounding base pairs (RNA-6 to RNA-11; Fig. 3*C* and *SI Appendix*, Fig. S8). (Note that we were unable to mutate the A bulge to a C as it caused structural rearrangement of the neighboring paired region.) If Synucleozid selectively binds to the 5′-G_G/3′-CAU (the A bulge and its closing pair, where underlining denotes the location of noncanonically paired or unpaired nucleotides), their mutation should all negatively impact binding. In contrast, mutation of the remaining noncanonically paired regions that are not putative Synucleozid binding sites should not significantly affect binding affinity.

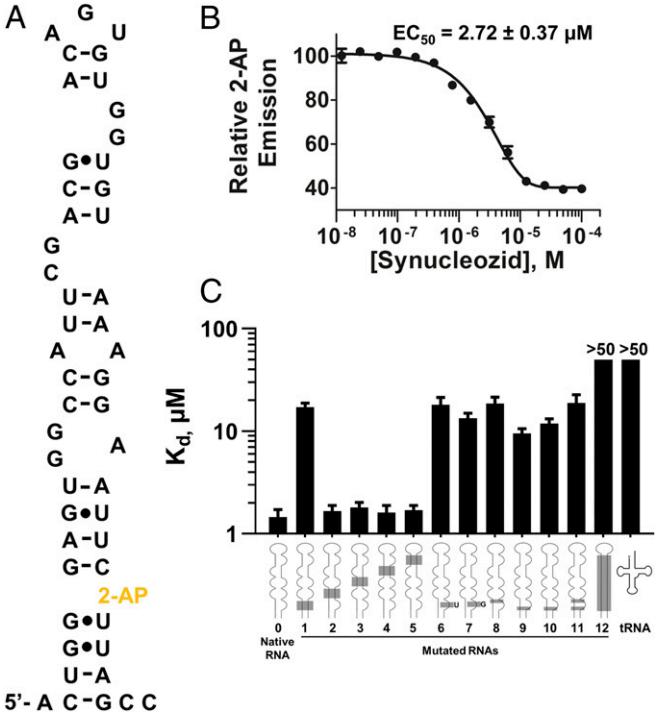

Fig. 3. Selectivity of Synucleozid for the A bulge in the *SNCA* IRE. (*A*) Secondary structure of 2-AP–labeled RNA used in the assays. (*B*) Plot of the change in 2-AP fluorescence as a function of Synucleozid concentration. (*C*) Plot of the affinity of Synucleozid for various *SNCA* IRE mutants as determined by competitive binding assays with the 2-AP–labeled RNA. RNA-0 is native *SNCA* IRE. RNA-12 is a fully base-paired RNA in which all 5 internal bulges and loops have been mutated. Each of RNA-1 to RNA-5 has 1 bulge or loop mutated. RNA-6 to RNA-12 are mutants of the A bulge or have mutated closing base pairs (*SI Appendix*, Figs. S7 and S8). Error bars indicate SD.

As expected, mutation of the A bulge to a base pair (RNA-1) or to a U or G bulge (RNA-6 and 7) reduced Synucleozid avidity by 10-fold as compared with the native IRE (K_d ~20 μM; Fig. 3*C* and *SI Appendix*, Fig. S7 *B* and *C*). Importantly, mutation of the closing base pairs (RNA-8 to 11) also reduced binding affinity, emphasizing the importance of the GC and GU closing base pairs in Synucleozid's molecular recognition of the native IRE (Fig. 3*C* and *SI Appendix*, Fig. S7*C*). Interestingly, the ferritin IRE has 3 U bulges and 1 C bulge (*SI Appendix*, Fig. S6). This 10-fold weaker binding observed to the U bulge, which might in part be traced to Synucleozid's doubly charged nature at physiological pH, could contribute to the observed reduction of ferritin protein levels (Fig. 2). Notably, as discussed above, the decreased ferritin levels observed upon Synucleozid treatment could also be due to rescue of an α-synuclein–mediated lysosomal dysfunction, as reduced ferritin levels were observed in α-synuclein$^{-/-}$ mice (35).

Replacement of all other noncanonically paired regions with base pairs (RNA-2 to 5) had no effect on Synucleozid binding, further indicating the selectivity of the compound for the A bulge. Two other RNAs were also studied in this competition assay: RNA-12, in which all internal loops and bulges, including the Synucleozid binding site, were replaced with base pairs, and tRNA. No significant recovery of the change in 2-AP emission was observed until >100 μM of either RNA was added (Fig. 3*C* and *SI Appendix*, Fig. S7*A*). To support these binding studies, thermal melting experiments were performed on the wild-type A-bulge IRE RNA and the corresponding fully paired RNA in the presence and absence of Synucleozid. The compound only stabilized the wild-type IRE upon binding, decreasing its $\Delta G_{37°C}$ from −2.91 to −3.23 kcal/mol and increasing its T_m by 3 °C (from 51.4 to 54.8 °C; *SI Appendix*, Fig. S9). Taken together with the binding studies on IRE mutants, these melting studies indicate that Synucleozid selectively recognizes the A bulge in the *SNCA* IRE, resulting in thermal stabilization of the target RNA.

To gain insight into the prevalence of the 5′-G_G/3′-CAU bulge that Synucleozid binds throughout the human transcriptome, we queried a database of secondary structural elements present in human miRNA hairpin precursors and highly expressed human RNAs with known structures (39). The latter include 5S rRNA, 16S rRNA, 23S rRNA, 7SL (signal recognition particle), RNase P RNA, U4/U6 snRNA, and 465 nonredundant tRNAs (2,459 total motifs). Among 7,436 motifs in miRNA hairpin precursors, 5′-G_G/3′-CAU only occurs twice, once in miR-1207 and once in miR-4310 (0.027%). The bulge only appears 3 times in highly expressed RNAs, each in a tRNA (0.12%). Further, various studies have shown that typically small molecules must target a functional site in order to induce downstream biological effects (26). We have previously shown that many factors affect the biological response of molecular recognition of an RNA target, including target abundance and molecular recognition of a functional site (26, 40). By analysis of these factors, the data support that targeting this 3-dimensional (3D) structure in the *SNCA* IRE selectively is indeed achievable and elicits a selective biological response.

Synucleozid Structure–Activity Relationships. To further investigate molecular recognition at the small-molecule level, a series of Synucleozid derivatives were synthesized and studied (*SI Appendix*, Fig. S10*A*). These compounds were designed to have improved blood–brain barrier (BBB) penetrance as defined by central nervous system multiparameter optimization (CNS MPO) scores (41). In particular, the guanidyl groups were replaced with imidazolyl or cyano groups, while functionalities within the heterocycle as well as the imino group linking the 2 benzyl substituents were altered to study how changes in hydrogen bonding and stacking capacity affect molecular recognition (*SI Appendix*, Fig. S10*A*).

Replacement of guanidyl groups with imidazolyl groups (SynucleoziD-2 to SynucleoziD-5) largely increased compound

CNS MPO scores without significantly affecting their avidity to the *SNCA* IRE as measured in the 2-AP fluorescence binding assay (*SI Appendix*, Fig. S10*B* and Table S2). Interestingly, despite the relatively small change in avidity, the cellular potency of all 4 derivatives was reduced compared with Synucleozid. At 1 μM concentration, Synucleozid reduced α-synuclein levels by ∼67%. In contrast, the 4 imidazolyl derivatives only reduced α-synuclein levels by ∼40% at 5 μM. Replacement of the guanidyl groups with cyano (SynucleoziD-NC) ablated both binding avidity and its inhibitory effect on *SNCA* mRNA translation (*SI Appendix*, Fig. S10*C* and Table S2). These findings suggest that Synucleozid can be further improved by using standard medicinal chemistry approaches.

Studying Molecular Recognition of Synucleozid to the *SNCA* IRE via ASO-Bind-Map. Traditionally, chemical mapping studies are used to identify ligand binding sites in vitro. However, compounds must be highly resident to detect their binding; that is, they must interact with the target site for sufficient time to inhibit an irreversible reaction with a chemical modification probe. Further confounding this analysis is that the sites that react with the modification reagent may not overlap with the ligand binding sites, leaving these sites invisible to detection (42). We previously developed various strategies (chemical cross-linking and isolation by pull-down to map binding sites [Chem-CLIP-Map] and small molecule–nucleic acid profiling by cleavage applied to RNA to map ligand binding sites [RiboSNAP-Map]) to alleviate these challenges and to extend mapping of ligand binding sites into cells (25, 42, 43). Although Chem-CLIP-Map and RiboSNAP-Map are powerful target-validation tools that demonstrate direct target engagement, they require the development of derivatives of lead compounds to attach a cross-linker or a cleavage moiety. Here, ASO-Bind-Map was developed to alleviate challenges associated with all 3 methods.

Previously, the Williamson laboratory explored the folding pathways of large, highly structured RNAs using a series of ASOs (44, 45). Domains within the RNA that fold quickly into stable structures were largely inaccessible to ASO binding and hence cleavage while ones that did not fold or folded more slowly were subjected to ASO-mediated cleavage. We adapted this approach to profile the binding sites of small molecules to RNAs both in vitro and in cellulis. That is, since Synucleozid stabilizes the IRE structure, it should impede ASO binding and reduce RNase H cleavage at the binding site (Fig. 4 and *SI Appendix*, Fig. S11).

After designing and validating 6 tiling ASOs that bind throughout the *SNCA* IRE hairpin structure (Fig. 4*A* and *SI Appendix*, Table S3), ASO-Bind-Map was implemented in 2 ways, using 1) a ^{32}P-labeled IRE and analysis by gel electrophoresis (Fig. 4*B*), and 2) a dually labeled IRE that is a fluorescence-based molecular beacon (Fig. 4*C*). In our first experiments, the ^{32}P-labeled IRE was incubated with 0.1, 1, and 10 μM Synucleozid followed by addition of ASO and then RNase H. As expected, protection of the IRE from RNase H cleavage by Synucleozid was only observed with ASOs whose binding sites overlap with the A bulge, namely ASO(1–10) and ASO(40–50) (Fig. 4*B* and *SI Appendix*, Fig. S11).

In the molecular beacon assay, a model of the *SNCA* IRE was dually labeled on the 5′ and 3′ ends with Cy3 and Cy5, respectively, a fluorescence resonance energy transfer (FRET) pair. Upon hybridization of an ASO, the hairpin unfolds and FRET is reduced. Again, if a small molecule is bound to a structure that overlaps with the sequence recognized by an ASO, the structure is stabilized, impeding ASO binding, and the extent of FRET reduction slows. Each ASO was validated for reducing FRET in this system (*SI Appendix*, Fig. S12). In agreement with the RNase H-mediated studies, Synucleozid was only able to reduce the extent of unfolding induced by ASO(1–10) and ASO(40–50), which bind sequences that overlap with the Synucleozid binding site, indicating specific binding to the A bulge (Fig. 4*C* and *SI Appendix*, Fig. S12).

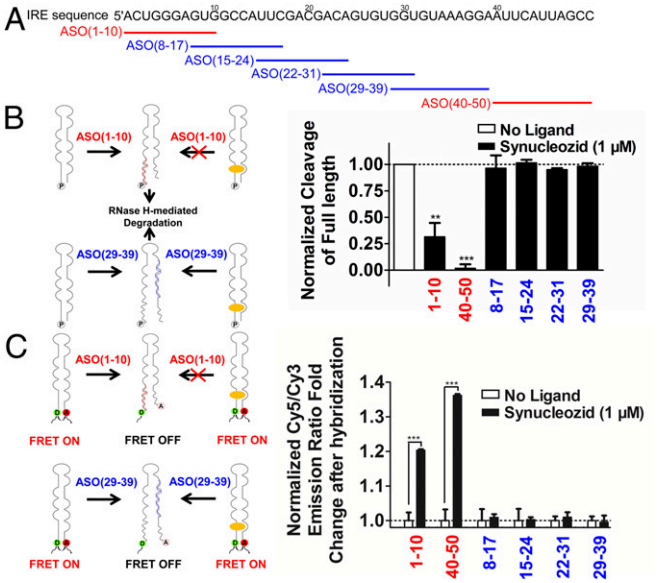

Fig. 4. ASO-Bind-Map studies confirm that Synucleozid binds to the predicted site in vitro and in cells. (*A*) Designed ASOs that tile through the *SNCA* IRE. (*B*, *Left*) Scheme of RNase H-mediated ASO-Bind-Map. (*B*, *Right*) Relative cleavage of full-length *SNCA* IRE by RNase H after hybridization of ASOs with or without Synucleozid preincubation. Statistical significance was calculated between each specific ASO with or without Synucleozid preincubation. (*C*, *Left*) Scheme of FRET-based ASO-Bind-Map. (*C*, *Right*) Normalized relative fold change of Cy5/Cy3 fluorescence for various ASOs with or without Synucleozid preincubation. $^{**}P < 0.01$, $^{***}P < 0.001$, as determined by a 2-tailed Student *t* test. Error bars indicate SD.

Collectively, these 3 different assays, 2-AP–labeled RNA (including mutational studies), RNase H-mediated ASO-Bind-Map, and molecular beacon ASO-Bind-Map, all support binding of Synucleozid to the A bulge as designed.

Profiling the Binding Site of Synucleozid in Cells via ASO-Bind-Map. To profile the binding of Synucleozid to the hairpin structure of the *SNCA* 5′ UTR in cells by ASO-Bind-MAP, ASO gapmers (2′-*O*-methoxyethyl [MOE] phosphorothioates) were used. Three oligonucleotides were studied: 1) the gapmer version of ASO(1–10), which overlaps with the Synucleozid binding site; 2) the gapmer version of ASO(29–39), which does not overlap with the Synucleozid binding site; and 3) a gapmer control ASO that does not share sequence complementarity with *SNCA* mRNA but has the same number and position of 2′-MOE modifications and is the same length as ASO(1–10) and ASO(29–39) (*SI Appendix*, Table S3).

Akin to in vitro studies, a gapmer of interest was transfected into SH-SY5Y cells in the presence and absence of Synucleozid (Fig. 5*A*). As expected, ASO(1–10) and ASO(29–39) (200 nM), but not the scrambled control ASO (200 nM), cleaved *SNCA* mRNA, reducing its levels by ∼50%, as measured by RT-qPCR. Addition of 0.1, 1, and 10 μM Synucleozid to cells afforded dose-dependent inhibition of *SNCA* mRNA cleavage by ASO(1–10), which binds the sequence in and around the A bulge, with an EC_{50} of 1 μM; no effect was observed with ASO(29–39) or the control ASO (Fig. 5*B*). These findings show direct target engagement in cells to further support that Synucleozid binds to the 3D structure in and around the A bulge in the *SNCA* 5′ UTR structure. Cellular engagement of the target at the designed site is an important step to validate a compound's mode of action.

Investigating the Cellular Mechanism of Action of Synucleozid. We investigated 3 potential mechanisms of action through which Synucleozid could inhibit α-synuclein translation: 1) Synucleozid

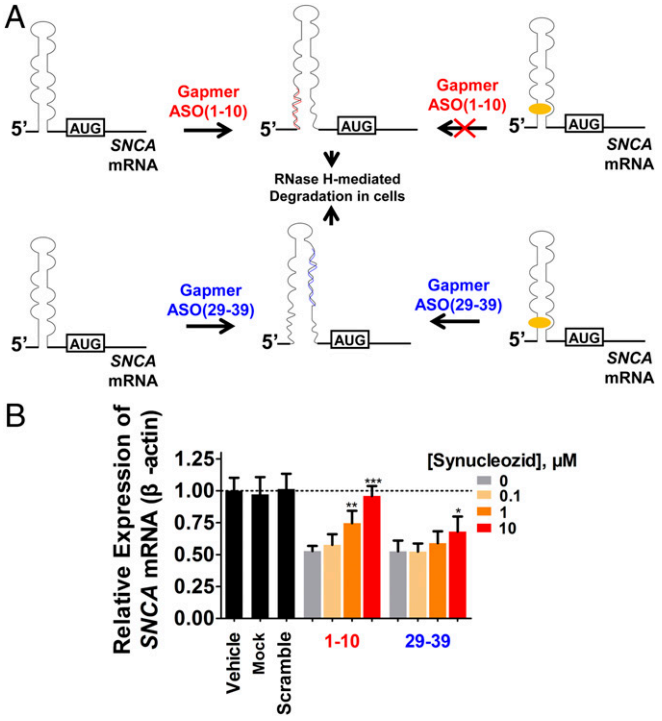

Fig. 5. Cellular ASO-Bind-Map validates the *SNCA* IRE as the target of Synucleozid. (*A*) Scheme of ASO-Bind-Map studies completed in cells. (*B*) Expression of *SNCA* mRNA in SH-SY5Y cells transfected with designed gapmers. Synucleozid protects *SNCA* mRNA from RNase H-mediated cleavage by ASO(1–10), which hybridizes with the Synucleozid binding site. Protection is not observed from cleavage mediated by ASO(29–39), which hybridizes to a distal site. $*P < 0.05$, $**P < 0.01$, $***P < 0.001$, as determined by ANOVA. Error bars indicate SD.

stabilizes the IRE hairpin structure and prevents its unfolding, and thus could block the preinitiation ribosome complex from scanning through the IRE portion of the mRNA and obstructing the assembly of translationally competent ribosome machinery (Fig. 6*A*); 2) Synucleozid could increase expression of the iron response element binding protein (IRP) and facilitate IRP and *SNCA* IRE complex formation (Fig. 7*A*); IRP–IRE complex formation leads to translational inhibition (20, 21); and 3) Synucleozid binding to the IRE could increase the affinity between IRP and IRE, consequently repressing translation (Fig. 7*A*).

We first investigated if Synucleozid affects ribosome assembly onto *SNCA* mRNA using polysome profiling. Polysome profiling is a powerful technique to study the association of mRNAs with ribosomes and to assess which mRNAs are undergoing active translation via their association in polysomes and the density of ribosomal loading (46). We collected polysomes in the presence and absence of Synucleozid and isolated them through a sucrose gradient (Fig. 6*B*, *Top*). Fractions of the polysomes as a function of the sucrose density gradient (e.g., the number of ribosomes loaded onto mRNAs) were collected, and the amount of *SNCA* mRNA relative to a control mRNA was measured by RT-qPCR (Fig. 6*B*, *Bottom*).

Indeed, treatment with Synucleozid alters the distribution of *SNCA* mRNA between incomplete ribosomes (association with 40S or 60S subunits; fractions 1 to 5), single ribosomes (80S; fractions 5 to 7), and polysomes (fractions 8 to 14) (Fig. 6 *B* and *C*), but does not affect the association of ribosomes with a control RNA. In particular, Synucleozid decreases the amount of *SNCA* mRNA associated with active polysomes by ∼20% ($P < 0.05$) with a concomitant increase in the amount associated with incomplete ribosomes ($P < 0.05$) (Fig. 6*C*). Canonical translation of eukaryotic mRNAs is initialized by recruiting the 40S ribosomal subunit to the 5′ cap (47). The 40S subunit and initiation factors form the preinitiation complex that scans from the 5′ end to the AUG start codon by unfolding the 5′ UTR, followed by recruitment of the 60S subunit. The complete 80S ribosome machinery then elongates through the open reading frame (ORF). The observed significant increase of mRNA in fractions 1 to 5 suggests that Synucleozid inhibits translation during the preinitiation complex scanning but not the elongation stage. Collectively, these findings in conjunction with the in vitro and in cellulis results from ASO-Bind-Map support the hypothesis that Synucleozid inhibits ribosomal loading onto the *SNCA* mRNA by stabilizing the IRE and preventing its unfolding.

We then studied if Synucleozid affects *SNCA* mRNA recognition by the 2 IRP isoforms, IRP-1 and IRP-2 (Fig. 7*A*). IRP-1 is an abundant protein that not only serves as an iron-responsive protein but also as an aconitase to catalyze the conversion of citrate to isocitrate (48). IRP-2 is a less abundant form and differs from IRP-1 by a 73-amino acid insertion, removing its aconitase activity and facilitating its degradation in cells with low iron levels (49). To exclude the possibility that Synucleozid affects IRP expression, SH-SY5Y cells were treated with Synucleozid, and IRP abundance was measured by Western blotting. No change in the levels of either protein was observed (*SI Appendix*, Fig. S13).

Next, IRP cellular complexes were isolated by immunoprecipitation (IP) and analyzed to assess if Synucleozid affects loading of IRPs onto the IRE of *SNCA* mRNA (Fig. 7*A*). A series of control experiments were completed for both IRP-1 and IRP-2 to ensure that differences in *SNCA* mRNA levels could be assayed (Fig. 7*B*). For IRP-1, treatment with iron (II) should decrease the amount of *SNCA* mRNA pulled down in the IP fractions, as iron (II) binds to IRP-1 and inhibits formation of the *SNCA* mRNA–IRP-1 complex, which was experimentally observed (Fig. 7*B*). As expected, the amount of pulled-down *SNCA* mRNA increased in the presence of the iron chelator deferoxamine (DFOA) (Fig. 7*B*). IRP-2 expression is dependent on iron (II) concentration (50). Therefore, as an experimental control, we treated cells with an ASO complementary to the IRP-2 binding site in the *SNCA* mRNA, which blocked IRP-2 binding and reduced the amount of immunoprecipitated *SNCA* mRNA (Fig. 7*B*). Importantly, Synucleozid did not affect the amount of *SNCA* mRNA associated with IRP-1 or IRP-2 in these carefully controlled IP experiments, consistent with in vitro displacement assays (Fig. 7*B* and *SI Appendix*, Fig. S14).

Collectively, these mechanistic investigations support a mechanism by which Synucleozid binds to the A-bulge 3D structure within the IRE hairpin of *SNCA* mRNA and inhibits the association of functional ribosomes with mRNA (Fig. 6*A*).

Proteome- and Transcriptome-Wide Studies to Evaluate Synucleozid Selectivity. To assess the proteome-wide selectivity of Synucleozid for reducing α-synuclein protein levels, we completed a series of studies comparing SH-SY5Y cells treated with 1) Synucleozid, 2) vehicle control, 3) α-synuclein small interfering (si)RNA, and 4) a scrambled control siRNA (*SI Appendix*, Fig. S15). Among the 3,300 proteins detected, 381 proteins (11%) were affected by α-synuclein siRNA treatment (relative to scrambled control siRNA-treated cells), while 283 (8%) of the proteins were significantly affected (adjusted $P < 0.01$) with the cell-permeable small molecule Synucleozid (relative to vehicle-treated cells) (Fig. 8 *A* and *B*; a spreadsheet of full proteomics analysis is provided in Dataset S1). Interestingly, the siRNA down-regulated 259 proteins (7.9% of all proteins) while Synucleozid down-regulated 143 (4.3% of all proteins), of which 53 overlap. The numbers of proteins with increased expression for the siRNA and Synucleozid are similar, 122 (3.7% of all proteins) and 140 (4.2% of all proteins), respectively, with 26 common proteins in the 2 datasets. These

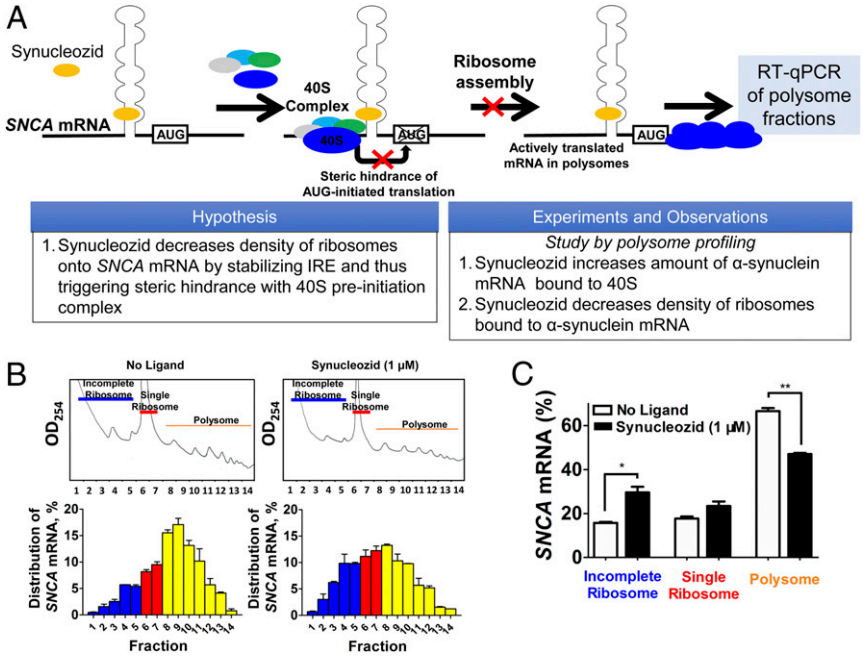

Fig. 6. Investigation of a potential mode of action of Synucleozid. (*A*) Synucleozid could affect the loading of *SNCA* mRNA into polysomes and/or the assembly of active ribosomes, which can be studied by polysome profiling. (*B*) Representative absorption trace (at 254 nm) of polysome fractionation from polysome profiling of SH-SY5Y cells treated with Synucleozid (1 μM) or vehicle (dimethyl sulfoxide; DMSO) (*Top*) and quantification of the percentage of *SNCA* mRNA level in each fraction relative to total *SNCA* mRNA expression, as assessed by RT-qPCR (*Bottom*). (*C*) Percentage of *SNCA* mRNA present within monosome- and polysome-containing fractions with (black) and without (white) Synucleozid (1 μM) treatment. Fractions labeled as "incomplete ribosome" contain 40S and 60S ribosomal subunits (fractions 1 to 5); "single ribosome" (fractions 6 and 7) indicates 80S ribosomes. $*P < 0.05$, $**P < 0.01$, as determined by a 2-tailed Student *t* test. Error bars indicate SD.

overlapping proteins could be involved in α-synuclein–related pathways. For example, previous studies indicated that α-synuclein impairs the mitochondrial complex in the brain (51, 52); thus, inhibition of α-synuclein synthesis could recover this phenotype. Indeed, down-regulation of α-synuclein by compound and siRNA treatment caused a common up-regulation of proteins involved in the oxidative phosphorylation pathway, such as ATP5B, NDUFS3, COX6B1, SDHA, and UQCRH (Fig. 8 *A* and *B*). Notably, we

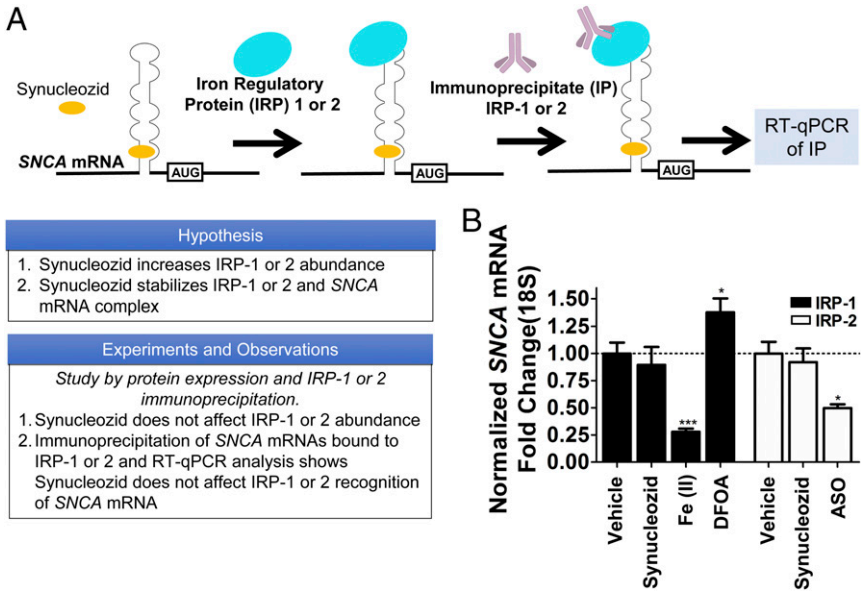

Fig. 7. Investigation of 2 other potential modes of action of Synucleozid. (*A*) Synucleozid could affect the abundance of IRPs and/or the affinity of the IRP–IRE complex, which can be assessed by Western blotting and immunoprecipitation. (*B*) *SNCA* mRNA was pulled down from treated (Synucleozid; 1 μM) and untreated (vehicle; DMSO) SH-SY5Y cells by immunoprecipitation of IRP-1 (black bars) or IRP-2 (white bars). *SNCA* mRNA levels were quantified by RT-qPCR. Iron (II) and deferoxamine are positive controls for IRP-1, and ASO is a positive control for IRP-2, each used to detect changes in the amount of immunoprecipitated mRNAs. The amount of *SNCA* mRNA bound to IRP-1 or IRP-2 shows no significant difference with or without Synucleozid treatment. $*P < 0.05$, $***P < 0.001$, as determined by a 2-tailed Student *t* test. Error bars indicate SD.

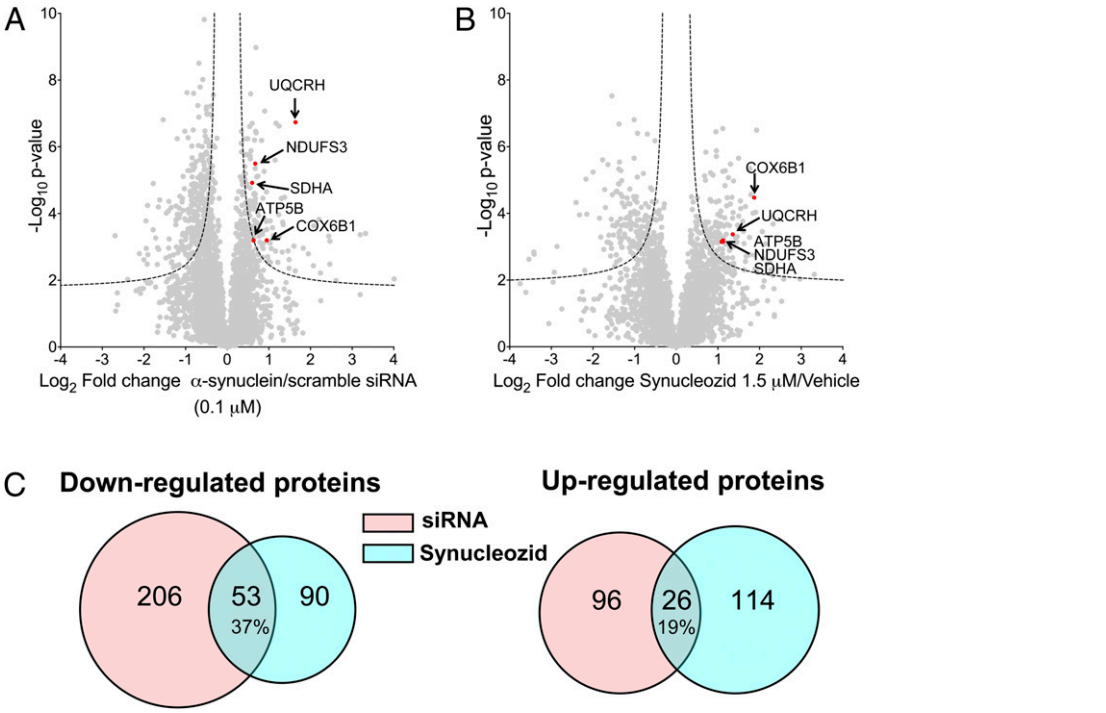

Fig. 8. Global proteome profiles of SH-SY5Y cells after treatment with Synucleozid or an siRNA directed at α-synuclein. (*A* and *B*) Volcano plots of SH-SY5Y cells treated with (*A*) α-synuclein siRNA vs. a scrambled control (0.1 μM), or (*B*) Synucleozid (1.5 μM) vs. vehicle are shown. Data are represented as $\log_2$ fold change; dotted lines represent a false discovery rate of 1% and an S_0 of 0.1, indicating an adjusted *P* value of 0.01. Red dots represent the common up-regulated proteins in the oxidative phosphorylation pathway. (*C*) Venn diagrams showing down- or up-regulated proteins upon α-synuclein siRNA or Synucleozid treatment compared with their respective controls.

searched for other proteins encoded by mRNAs with IREs in proteomics data ($n = 16$; Dataset S1), 4 of which were expressed at measurable levels: ACO2, NDUFS1, CDC42BPB, and FTH1 (ferritin). Only FTH1 was affected by Synucleozid treatment, as expected from the cellular studies presented in Fig. 2. In summary, Synucleozid demonstrated proteome-wide selectivity, which indicates targeting the *SNCA* IRE by small molecules is a promising direction for drug discovery and development since off-target effects have been previously observed in nucleic acid-based knockdown experiments (53).

In complementary studies, we examined the transcriptome-wide effect of Synucleozid treatment using RNA-seq (54). Differentially expressed genes were identified using quantification and analyses from the Kallisto and Sleuth packages in R (29). Very few changes were observed upon Synucleozid (19,979/20,034 genes were unchanged; 99.7%) or siRNA treatment (19,279/19,329 genes were unchanged; 99.7%), suggesting limited off-target effects for either modality (*SI Appendix*, Fig. S16).

Comparisons with Other Compounds That Target RNA. Previously, a high-throughput screen was used to identify inhibitors of α-synuclein translation, including plant cardiac glycosides, mycophenolic acid (an immunosuppressant and iron chelator), and posiphen (55). Although these compounds were found to selectively inhibit α-synuclein production, their mechanism of action is unknown. Synucleozid, however, establishes that small molecules can recognize the *SNCA* 5′ UTR IRE in cells, affecting assembly of mature ribosomes onto the mRNA. Given that we have established this mechanism of action in cells and the observation that many other proteins that are overexpressed in neurological disorders have IREs in their 5′ UTRs, such an approach and the strategies described herein could be broadly applied to other proteins, particularly APP, which is up-regulated in Alzheimer's disease and Down's syndrome patients' brains (56). These IREs have different 3D structures that could be targeted selectively by different small molecules that could be identified through sequence-based design.

Additionally, small molecules have been shown to activate or inhibit translation in RNA repeating transcripts. For example, the toxicity observed in fragile X-associated tremor ataxia syndrome, and C9orf72-associated frontotemporal dementia and amyotrophic lateral sclerosis, is caused in part by repeat associated non-ATG (RAN) translation of expanded r(CGG) and r(G_4C_2) repeating transcripts, respectively (57, 58). Small molecules that bind to these structures inhibit cellular RAN translation by directly binding to the repeats and affecting loading of the RNAs into polysomes. However, in these cases, the repeat sequence itself is being translated. The highly repeating nature of these targets allows for higher loading of compounds compared with the IRE described herein. Thus, it is encouraging that translation can be inhibited by binding to a single site in the 5′ UTR to impede ribosome assembly.

Other small molecules can target human RNAs and modulate their biology by affecting RNA–protein complexes. For example, small molecules have been designed to target miRNA precursors to inhibit their biogenesis and derepress downstream protein targets (59–62). Viral RNAs have been important targets of small molecules by using both screening and rational design to inhibit viral transcription and translation (63–65). Collectively, there are many avenues to affect RNA biology, that is, through inhibition of RNA–protein complexes and binding to functional sites in an RNA. Not all sites of an RNA that are targetable with small molecules are functional and, thus, are unlikely to elicit a cellular response (26). Importantly, these studies show that small molecules that bind to structural elements in 5′ UTRs proximal to start codons can affect ribosome assembly in a selective fashion, and we show that these sites can be considered functional.

Many Intrinsically Disordered Proteins Are Encoded by Intrinsically Ordered or Structured mRNAs That Could Be Drugged with Small Molecules. Previous in silico studies of the human genome as well as a focused analysis of the *MYC* mRNA suggest that targetable secondary structures may be common in human genes (66, 67). To assess structural propensity in *SNCA* and mRNAs encoding other IDPs, all sequences from DisProt (68), a database of IDPs, were analyzed using the ScanFold pipeline (69), previously used for the human genome and *MYC* mRNA (61). Briefly, ScanFold uses a scanning analysis window to predict the most stable folds across each mRNA as well as metrics that suggest sequences that may be ordered, presumably by evolution, to be particularly stable. Stability is quantified by the thermodynamic z score; lower z scores indicate that a sequence is ordered to adopt a more stable secondary structure than expected for its particular nucleotide composition. Unique consensus structures from overlapping sequence windows are generated by weighting the base pairs that most contribute to these unusually stable secondary structures. A summary of the results is shown in *SI Appendix*, Fig. S17, and all results are available on Zenodo (70).

We analyzed if each mRNA is globally ordered by calculating the average z score for having stable structures across all windows of each mRNA. If the average of all windows is <-1, the transcript is deemed to be globally ordered (71). The mean average z score for all mRNAs encoding IDPs, which was normally distributed, was −0.51 (*SI Appendix*, Table S4). Overall, few mRNAs (13/236; 5.5%) were considered globally ordered. *SNCA* was not particularly biased for global structure, as indicated by its average z score of −0.37. Of the mRNAs encoding the IDPs studied, ∼30% were expected to be even less ordered (as indicated by higher and in some cases even positive z scores; *SI Appendix*, Fig. S17).

Interestingly, all mRNAs studied, whether or not classified as globally ordered, had regions with defined structures. That is, in each mRNA that encodes for an IDP, there is a particular set of windows with z score(s) <-1 where unusually stable base pairs reside. These regions form loops, bulges, and other structures that are attractive targets for RNA-binding molecules (*SI Appendix*, Fig. S17). For example, 36% of *SNCA*'s 3,167 nt contribute to structures that generate z scores with values <-1. Notably, none of the *SNCA* IRE base pairs is predicted to be significantly more stable than expected as compared with random sequences (70), which may not be surprising, as a degree of structural flexibility may be required to accommodate interactions with IRPs and was observed experimentally in our mapping studies (*SI Appendix*, Fig. S1*B*). Similar results were observed for the viral structured ncRNA HSUR1, which requires structural flexibility to allow interactions with host biomolecules (72). Collectively, these results indicate that our approach to targeting undruggable proteins by targeting structures in the encoding mRNA could be successfully applied to other IDP-encoding mRNAs.

Conclusions and Implications. The present set of studies demonstrates the feasibility of down-regulating α-synuclein protein levels by selectively targeting its mRNA 5′ UTR with the small molecule Synucleozid. Global proteomics and RNA-seq studies showed that Synucleozid is selective proteome-wide and transcriptome-wide. Thus, these findings provide a promising approach for achieving disease modification in α-synuclein–associated neurodegenerative disorders including Parkinson's disease and dementia with Lewy bodies.

There is a myriad of RNA structures throughout the transcriptome that may be targetable with small molecules to modulate RNA biology (*SI Appendix*, Fig. S17). The studies herein further illustrate that sequence-based design can rapidly identify compounds that bind an RNA target. Our ASO-Bind-Map strategy not only validates the target of the small molecule but also if it binds the intended site. Indeed, such target-validation studies are essential to define the compound mode of action, namely that cellular occupancy of the target is leading to the observed biological effect.

The tool compounds developed here could serve as drug leads or useful entry points for medicinal chemistry studies to optimize properties such as BBB penetrance and to mitigate off-target liabilities. In support of this, our structure–activity relationship studies provided compounds that retained activity with improved likelihood of BBB penetrance, as predicted by CNS MPO calculations. Additionally, the ability to design small molecules with selectivities that are competitive with, if not exceed, those of siRNAs suggests that small-molecule targeting of RNA could be a sustained approach to affect biology for therapeutic benefit. Selectivity is derived from small-molecule recognition of a particular RNA 3D fold and could be further enhanced by designing compounds that interact with multiple motifs within an RNA target simultaneously (6, 73–75).

We showed mechanistically that Synucleozid affects α-synuclein translation by directly affecting the RNA and not an RNA–protein complex. Key to small-molecule bioactivity for RNA targets is binding to a functional site. By using ASO-Bind-Map coupled with mechanistic investigations, our studies show that ligand binding to a 3D structure proximal to a start codon can affect ribosome assembly onto the mRNA. This cellular activity is distinct from previous studies on drugging RNA in cells and sets the stage for broadening the use of small molecules to affect canonical translation. Many disease-causing proteins are encoded by RNAs that have conserved structures in their UTRs, for example, Huntingtin mRNA (76, 77), that could be targeted to inhibit their translation. Thus, this approach may not be limited to mRNAs with IREs and is particularly intriguing for proteins lacking traditional, druggable folds. Importantly, our studies indicate that mRNAs encoding IDPs are structured, providing a route to inhibit proteins that are difficult to target with small molecules.

Materials and Methods

Detailed information for all experimental methods and materials, including synthetic methods and compound characterization, is provided in *SI Appendix*.

Statistical Analysis. Data are presented as means ± SD from at least 3 independent biological replicates. Statistical significance between experimental groups was analyzed either by 2-tailed Student t test or one-way ANOVA followed by Bonferroni's multiple-comparison test. In all cases, P values of less than 0.05 were considered to be statistically significant.

Cell Culture. Please see *SI Appendix* for details.

Reverse Transcription-Quantitative Real-Time PCR (RT-qPCR). After completion of treatment, total RNA was extracted from cells (RNeasy Mini Kit; Qiagen) and cDNA was synthesized (Superscript II; Invitrogen) according to the manufacturer's instructions. Quantitative real-time PCR was performed in triplicate using iTaq Universal SYBR Green Supermix (Bio-Rad) with the Applied Biosystems 7500 Real-Time PCR System to assess the relative *SNCA* mRNA levels. Please see *SI Appendix* for additional details including primer sequences.

Western Blotting. Protein expression of α-synuclein, APP, ferritin, and TfR were analyzed in SH-SY5Y cells, while the level of PrP was tested in Neuro-2A cells after compound or vehicle treatment. To improve immunodetection of endogenous α-synuclein, membranes used to probe for endogenous α-synuclein were mildly fixed with 0.4% paraformaldehyde for 30 min at room temperature prior to the blocking step (78). Additional details are provided in *SI Appendix*.

Cell-Death Assay. The cytoprotective effect of Synucleozid was tested against α-synuclein PFFs. Human α-synuclein was expressed (79) and fibrillization was induced as previously described (80). SH-SY5Y cells were pretreated with Synucleozid (0.25 to 1 μM) for 24 h and challenged with 50 μg/mL

α-synuclein PFFs for an additional 48 h in the presence of Synucleozid. Cell death was measured using an LDH Cytotoxicity Detection Kit (Takara) according to the manufacturer's instructions and plotted either as optical density value or as percent changes in comparison with the respective controls. Monomeric α-synuclein (50 μg/mL) challenge was used as negative control for PFF cytotoxicity. Additional details are provided in *SI Appendix*.

To assess if Synucleozid has a cytotoxic effect, SH-SY5Y cells were treated with 0.25 to 1 μM for 48 h, and cell viability and cytotoxicity were measured using the CellTiter 96 AQueous One Solution Cell Proliferation Assay (MTS) (Promega) according to the manufacturer's instructions.

Data Availability. RNA-seq data are available in the Gene Expression Omnibus (GEO) repository (accession no. GSE129590; ref. 54).

ACKNOWLEDGMENTS. This work was funded by NIH Grants IGNITE R21/R33 NS096032 (to M.M.M. and M.D.D.), R01GM97455 and DP1NS096898 (to M.D.D.), and R00 GM112877 and R01GM133810 (to W.N.M.). We also thank the Nelson Family Fund. Additionally, M.M.M. is the William Dow Lovett Professor of Neurology and is supported by the Michael J. Fox Foundation for Parkinson's Research, American Parkinson Disease Association, New Jersey Health Foundation, and NIH Grants AT006868, NS073994, and NS101134. E.J. is supported by NIH Grants NS070898 and NS095003 and by the State of New Jersey.

1. M. Clamp *et al.*, Distinguishing protein-coding and noncoding genes in the human genome. *Proc. Natl. Acad. Sci. U.S.A.* **104**, 19428–19433 (2007).
2. A. L. Hopkins, C. R. Groom, The druggable genome. *Nat. Rev. Drug Discov.* **1**, 727–730 (2002).
3. C. V. Dang, E. P. Reddy, K. M. Shokat, L. Soucek, Drugging the 'undruggable' cancer targets. *Nat. Rev. Cancer* **17**, 502–508 (2017).
4. J. Spiegel, P. M. Cromm, G. Zimmermann, T. N. Grossmann, H. Waldmann, Small-molecule modulation of Ras signaling. *Nat. Chem. Biol.* **10**, 613–622 (2014).
5. S. P. Velagapudi, S. M. Gallo, M. D. Disney, Sequence-based design of bioactive small molecules that target precursor microRNAs. *Nat. Chem. Biol.* **10**, 291–297 (2014).
6. S. P. Velagapudi *et al.*, Design of a small molecule against an oncogenic noncoding RNA. *Proc. Natl. Acad. Sci. U.S.A.* **113**, 5898–5903 (2016).
7. V. M. Lee, J. Q. Trojanowski, Mechanisms of Parkinson's disease linked to pathological alpha-synuclein: New targets for drug discovery. *Neuron* **52**, 33–38 (2006).
8. M. G. Spillantini *et al.*, Alpha-synuclein in Lewy bodies. *Nature* **388**, 839–840 (1997).
9. K. C. Luk *et al.*, Pathological α-synuclein transmission initiates Parkinson-like neurodegeneration in nontransgenic mice. *Science* **338**, 949–953 (2012).
10. E. Junn, M. M. Mouradian, Human alpha-synuclein over-expression increases intracellular reactive oxygen species levels and susceptibility to dopamine. *Neurosci. Lett.* **320**, 146–150 (2002).
11. E. Rockenstein *et al.*, Accumulation of oligomer-prone α-synuclein exacerbates synaptic and neuronal degeneration in vivo. *Brain* **137**, 1496–1513 (2014).
12. A. B. Singleton *et al.*, Alpha-synuclein locus triplication causes Parkinson's disease. *Science* **302**, 841 (2003).
13. D. M. Maraganore *et al.*; Genetic Epidemiology of Parkinson's Disease (GEO-PD) Consortium, Collaborative analysis of alpha-synuclein gene promoter variability and Parkinson disease. *JAMA* **296**, 661–670 (2006).
14. J. Fuchs *et al.*, Genetic variability in the SNCA gene influences alpha-synuclein levels in the blood and brain. *FASEB J.* **22**, 1327–1334 (2008).
15. F. Soldner *et al.*, Parkinson-associated risk variant in distal enhancer of α-synuclein modulates target gene expression. *Nature* **533**, 95–99 (2016).
16. E. Junn *et al.*, Repression of alpha-synuclein expression and toxicity by microRNA-7. *Proc. Natl. Acad. Sci. U.S.A.* **106**, 13052–13057 (2009).
17. D. M. Maraganore, Rationale for therapeutic silencing of alpha-synuclein in Parkinson's disease. *J. Mov. Disord.* **4**, 1–7 (2011).
18. A. L. Friedlich, R. E. Tanzi, J. T. Rogers, The 5′-untranslated region of Parkinson's disease alpha-synuclein messengerRNA contains a predicted iron responsive element. *Mol. Psychiatry* **12**, 222–223 (2007).
19. F. Febbraro, M. Giorgi, S. Caldarola, F. Loreni, M. Romero-Ramos, α-Synuclein expression is modulated at the translational level by iron. *Neuroreport* **23**, 576–580 (2012).
20. J. S. McDowall, D. R. Brown, Alpha-synuclein: Relating metals to structure, function and inhibition. *Metallomics* **8**, 385–397 (2016).
21. Z. D. Zhou, E. K. Tan, Iron regulatory protein (IRP)-iron responsive element (IRE) signaling pathway in human neurodegenerative diseases. *Mol. Neurodegener.* **12**, 75 (2017).
22. D. Olivares, X. Huang, L. Branden, N. H. Greig, J. T. Rogers, Physiological and pathological role of alpha-synuclein in Parkinson's disease through iron mediated oxidative stress; the role of a putative iron-responsive element. *Int. J. Mol. Sci.* **10**, 1226–1260 (2009).
23. R. J. Castellani, S. L. Siedlak, G. Perry, M. A. Smith, Sequestration of iron by Lewy bodies in Parkinson's disease. *Acta Neuropathol.* **100**, 111–114 (2000).
24. M. D. Disney *et al.*, Inforna 2.0: A platform for the sequence-based design of small molecules targeting structured RNAs. *ACS Chem. Biol.* **11**, 1720–1728 (2016).
25. S. G. Rzuczek *et al.*, Precise small-molecule recognition of a toxic CUG RNA repeat expansion. *Nat. Chem. Biol.* **13**, 188–193 (2017).
26. M. G. Costales *et al.*, Small molecule inhibition of microRNA-210 reprograms an oncogenic hypoxic circuit. *J. Am. Chem. Soc.* **139**, 3446–3455 (2017).
27. J. L. Childs-Disney *et al.*, A massively parallel selection of small molecule-RNA motif binding partners informs design of an antiviral from sequence. *Chem* **4**, 2384–2404 (2018).
28. D. R. Zerbino *et al.*, Ensembl 2018. *Nucleic Acids Res.* **46**, D754–D761 (2018).
29. H. Pimentel, N. L. Bray, S. Puente, P. Melsted, L. Pachter, Differential analysis of RNA-seq incorporating quantification uncertainty. *Nat. Methods* **14**, 687–690 (2017).
30. J. T. Rogers *et al.*, The alpha-synuclein 5′untranslated region targeted translation blockers: Anti-alpha synuclein efficacy of cardiac glycosides and posiphen. *J. Neural Transm. (Vienna)* **118**, 493–507 (2011).
31. I. Kalvari *et al.*, Rfam 13.0: Shifting to a genome-centric resource for non-coding RNA families. *Nucleic Acids Res.* **46**, D335–D342 (2018).
32. L. A. Volpicelli-Daley *et al.*, Exogenous α-synuclein fibrils induce Lewy body pathology leading to synaptic dysfunction and neuron death. *Neuron* **72**, 57–71 (2011).
33. D. N. Rupani, G. J. Connell, Transferrin receptor mRNA interactions contributing to iron homeostasis. *RNA* **22**, 1271–1282 (2016).
34. J. R. Mazzulli, F. Zunke, O. Isacson, L. Studer, D. Krainc, α-Synuclein-induced lysosomal dysfunction occurs through disruptions in protein trafficking in human midbrain synucleinopathy models. *Proc. Natl. Acad. Sci. U.S.A.* **113**, 1931–1936 (2016).
35. S. Baksi, N. Singh, α-Synuclein impairs ferritinophagy in the retinal pigment epithelium: Implications for retinal iron dyshomeostasis in Parkinson's disease. *Sci. Rep.* **7**, 12843 (2017).
36. J. M. Jean, K. B. Hall, 2-Aminopurine fluorescence quenching and lifetimes: Role of base stacking. *Proc. Natl. Acad. Sci. U.S.A.* **98**, 37–41 (2001).
37. M. Kaul, C. M. Barbieri, D. S. Pilch, Fluorescence-based approach for detecting and characterizing antibiotic-induced conformational changes in ribosomal RNA: Comparing aminoglycoside binding to prokaryotic and eukaryotic ribosomal RNA sequences. *J. Am. Chem. Soc.* **126**, 3447–3453 (2004).
38. S. Shandrick *et al.*, Monitoring molecular recognition of the ribosomal decoding site. *Angew. Chem. Int. Ed. Engl.* **43**, 3177–3182 (2004).
39. B. Liu *et al.*, Analysis of secondary structural elements in human microRNA hairpin precursors. *BMC Bioinformatics* **17**, 112 (2016).
40. M. D. Disney, Targeting RNA with small molecules to capture opportunities at the intersection of chemistry, biology, and medicine. *J. Am. Chem. Soc.* **141**, 6776–6790 (2019).
41. T. T. Wager, X. Hou, P. R. Verhoest, A. Villalobos, Central nervous system multiparameter optimization desirability: Application in drug discovery. *ACS Chem. Neurosci.* **7**, 767–775 (2016).
42. M. D. Disney, B. G. Dwyer, J. L. Childs-Disney, Drugging the RNA world. *Cold Spring Harb. Perspect. Biol.* **10**, a034769 (2018).
43. W. Y. Yang, H. D. Wilson, S. P. Velagapudi, M. D. Disney, Inhibition of non-ATG translational events in cells via covalent small molecules targeting RNA. *J. Am. Chem. Soc.* **137**, 5336–5345 (2015).
44. P. P. Zarrinkar, J. Wang, J. R. Williamson, Slow folding kinetics of RNase P RNA. *RNA* **2**, 564–573 (1996).
45. P. P. Zarrinkar, J. R. Williamson, Kinetic intermediates in RNA folding. *Science* **265**, 918–924 (1994).
46. H. Chassé, S. Boulben, V. Costache, P. Cormier, J. Morales, Analysis of translation using polysome profiling. *Nucleic Acids Res.* **45**, e15 (2017).
47. C. Peña, E. Hurt, V. G. Panse, Eukaryotic ribosome assembly, transport and quality control. *Nat. Struct. Mol. Biol.* **24**, 689–699 (2017).
48. R. S. Eisenstein, Iron regulatory proteins and the molecular control of mammalian iron metabolism. *Annu. Rev. Nutr.* **20**, 627–662 (2000).
49. M. W. Hentze, L. C. Kühn, Molecular control of vertebrate iron metabolism: mRNA-based regulatory circuits operated by iron, nitric oxide, and oxidative stress. *Proc. Natl. Acad. Sci. U.S.A.* **93**, 8175–8182 (1996).
50. B. Guo, J. D. Phillips, Y. Yu, E. A. Leibold, Iron regulates the intracellular degradation of iron regulatory protein 2 by the proteasome. *J. Biol. Chem.* **270**, 21645–21651 (1995).
51. L. Devi, V. Raghavendran, B. M. Prabhu, N. G. Avadhani, H. K. Anandatheerthavarada, Mitochondrial import and accumulation of alpha-synuclein impair complex I in human dopaminergic neuronal cultures and Parkinson disease brain. *J. Biol. Chem.* **283**, 9089–9100 (2008).
52. G. Liu *et al.*, Alpha-synuclein is differentially expressed in mitochondria from different rat brain regions and dose-dependently down-regulates complex I activity. *Neurosci. Lett.* **454**, 187–192 (2009).
53. L. Stojic *et al.*, Specificity of RNAi, LNA and CRISPRi as loss-of-function methods in transcriptional analysis. *Nucleic Acids Res.* **46**, 5950–5966 (2018).
54. P. Zhang *et al.*, Studying the selectivity of a small molecule Synucleozid on transcriptome. Gene Expression Omnibus. https://www.ncbi.nlm.nih.gov/geo/query/acc.cgi?acc=GSE129590. Deposited 11 December 2019.
55. S. Bandyopadhyay *et al.*, Novel 5′ untranslated region directed blockers of iron-regulatory protein-1 dependent amyloid precursor protein translation: Implications for Down syndrome and Alzheimer's disease. *PLoS One* **8**, e65978 (2013).
56. B. Rumble *et al.*, Amyloid A4 protein and its precursor in Down's syndrome and Alzheimer's disease. *N. Engl. J. Med.* **320**, 1446–1452 (1989).
57. Z. Su *et al.*, Discovery of a biomarker and lead small molecules to target r(GGGGCC)-associated defects in c9FTD/ALS. *Neuron* **83**, 1043–1050 (2014).
58. W. Y. Yang *et al.*, Small molecule recognition and tools to study modulation of $r(CGG)^{exp}$ in fragile X-associated tremor ataxia syndrome. *ACS Chem. Biol.* **11**, 2456–2465 (2016).
59. D. D. Vo, M. Duca, Design of multimodal small molecules targeting miRNAs biogenesis: Synthesis and in vitro evaluation. *Methods Mol. Biol.* **1517**, 137–154 (2017).
60. D. D. Vo *et al.*, Building of neomycin-nucleobase-amino acid conjugates for the inhibition of oncogenic miRNAs biogenesis. *Org. Biomol. Chem.* **16**, 6262–6274 (2018).
61. A. Murata, T. Otabe, J. Zhang, K. Nakatani, BzDANP, a small-molecule modulator of pre-miR-29a maturation by Dicer. *ACS Chem. Biol.* **11**, 2790–2796 (2016).

62. A. Murata, Y. Harada, T. Fukuzumi, K. Nakatani, Fluorescent indicator displacement assay of ligands targeting 10 microRNA precursors. *Bioorg. Med. Chem.* **21**, 7101–7106 (2013).
63. A. Davidson *et al*., Simultaneous recognition of HIV-1 TAR RNA bulge and loop sequences by cyclic peptide mimics of Tat protein. *Proc. Natl. Acad. Sci. U.S.A.* **106**, 11931–11936 (2009).
64. F. Hamy *et al*., An inhibitor of the Tat/TAR RNA interaction that effectively suppresses HIV-1 replication. *Proc. Natl. Acad. Sci. U.S.A.* **94**, 3548–3553 (1997).
65. R. Tan, L. Chen, J. A. Buettner, D. Hudson, A. D. Frankel, RNA recognition by an isolated alpha helix. *Cell* **73**, 1031–1040 (1993).
66. R. J. Andrews, L. Baber, W. N. Moss, RNAStructuromeDB: A genome-wide database for RNA structural inference. *Sci. Rep.* **7**, 17269 (2017).
67. C. A. O'Leary *et al*., RNA structural analysis of the MYC mRNA reveals conserved motifs that affect gene expression. *PLoS One* **14**, e0213758 (2019).
68. M. Sickmeier *et al*., DisProt: The database of disordered proteins. *Nucleic Acids Res.* **35**, D786–D793 (2007).
69. R. J. Andrews, J. Roche, W. N. Moss, ScanFold: An approach for genome-wide discovery of local RNA structural elements—Applications to Zika virus and HIV. *PeerJ* **6**, e6136 (2018).
70. W. N. Moss, Data from "Dataset S2." Zenodo. https://zenodo.org/record/3594202#.Xgabv43CFiC. Deposited 27 December 2019.
71. M. Davis, S. M. Sagan, J. P. Pezacki, D. J. Evans, P. Simmonds, Bioinformatic and physical characterizations of genome-scale ordered RNA structure in mammalian RNA viruses. *J. Virol.* **82**, 11824–11836 (2008).
72. P. Pawlica, W. N. Moss, J. A. Steitz, Host miRNA degradation by *Herpesvirus saimiri* small nuclear RNA requires an unstructured interacting region. *RNA* **22**, 1181–1189 (2016).
73. M. M. Lee, J. M. French, M. D. Disney, Influencing uptake and localization of aminoglycoside-functionalized peptoids. *Mol. Biosyst.* **7**, 2441–2451 (2011).
74. J. L. Childs-Disney, P. B. Tsitovich, M. D. Disney, Using modularly assembled ligands to bind RNA internal loops separated by different distances. *Chembiochem* **12**, 2143–2146 (2011).
75. V. Bernat, M. D. Disney, RNA structures as mediators of neurological diseases and as drug targets. *Neuron* **87**, 28–46 (2015).
76. J. Lee *et al*., An upstream open reading frame impedes translation of the huntingtin gene. *Nucleic Acids Res.* **30**, 5110–5119 (2002).
77. J. Pelletier, N. Sonenberg, Insertion mutagenesis to increase secondary structure within the 5′ noncoding region of a eukaryotic mRNA reduces translational efficiency. *Cell* **40**, 515–526 (1985).
78. B. R. Lee, T. Kamitani, Improved immunodetection of endogenous α-synuclein. *PLoS One* **6**, e23939 (2011).
79. P. H. Weinreb, W. Zhen, A. W. Poon, K. A. Conway, P. T. Lansbury , Jr, NACP, a protein implicated in Alzheimer's disease and learning, is natively unfolded. *Biochemistry* **35**, 13709–13715 (1996).
80. R. Yan *et al*., Synergistic neuroprotection by coffee components eicosanoyl-5-hydroxytryptamide and caffeine in models of Parkinson's disease and DLB. *Proc. Natl. Acad. Sci. U.S.A.* **115**, E12053–E12062 (2018).